Implications of thermo-chemical instability on the contracted modes in CO_2 microwave plasmas

A.J. Wolf[1], T.W.H. Righart[1], F.J.J. Peeters[1], W.A. Bongers[1], and M.C.M van de Sanden[1,2]

[1]DIFFER - Dutch Institute for Fundamental Energy Research, De Zaale 20, 5612AJ Eindhoven, The Netherlands
[2]Department of Applied Physics, Eindhoven University of Technology, P.O Box 513, 5600 MB Eindhoven, The Netherlands

December 2019

Abstract

Understanding and control over plasma instabilities and contraction phenomena in reactive flows is essential to optimize the discharge parameters for plasma processing applications such as fuel reforming and gas conversion. In this work, we describe the characteristic discharge modes in a CO_2 microwave plasma and assess the impact of wave coupling and thermal reactivity on the contraction dynamics. The plasma shape and gas temperature are obtained from the emission profile and the Doppler broadening of the 777 nm O(^{5}S $\leftarrow$ ^{5}P) oxygen triplet, respectively. Based on these observations, three distinct discharge modes are identified in the pressure range of 10 mbar to atmospheric pressure. We find that discharge contraction is suppressed by an absorption cut-off of the microwave field at the critical electron density, resulting in a homogeneous discharge mode below the critical transition pressure of 85 mbar. Further increase in the pressure leads to two contracted discharge modes, one emerging at a temperature of 3000 to 4000 K and one at a temperature of 6000 to 7000 K, which correspond to the thermal dissociation thresholds of CO_2 and CO respectively. The transition dynamics are explained by a thermo-chemical instability, which arises from the coupling of the thermal-ionization instability to heat transfer resulting from thermally driven endothermic CO_2 dissociation reactions. These results highlight the impact of thermal chemistry on the contraction dynamics of reactive molecular plasmas.

Keywords: carbon dioxide, solar fuels, microwave plasma, reactive plasma, thermal conversion, thermal instability, chemical instability

1 Introduction

Plasmas in reactive flows have been widely studied for a range of plasma-chemical processing applications such as plasma-catalysis[33,44], fuel reforming[11], and plasma-conversion of stable molecules such as CO_2, H_2O and N_2 for the production of synthetic fuels and value-added chemicals[38,42]. Discharge contraction phenomena are common in such discharges, enhanced by both the molecular nature[31] and the moderate to atmospheric pressure conditions often required in such processing applications. Distinct homogeneous and contracted modes emerge as the equilibrated states of plasma instabilities, each resulting in distinct discharge parameters and, subsequently, plasma-chemical processing conditions. A thorough understanding of the underlying contraction mechanisms is required to aid the development and optimization of plasma-assisted processing, synthesis, and conversion processes.

Microwave plasma-driven conversion of CO_2, aimed at producing CO feedstock for synthetic fuels[42], is a currently relevant topic of research, motivated by the rising concerns of global warming. Discharge contraction has proven to play an essential role in optimization of the reactor performance. Energy efficiency values of 70-80 % have been reported in a vortex stabilized discharge configuration. The optimal conditions were reported to coincide with a plasma transition from a diffuse to contracted discharge mode, under hypothesized conditions of strong vibrational-translational (VT) non-equilibrium around 160 mbar[1,6,16] for a power of 1400 W and a CO_2 flow rate of 24 slm. Subsequent investigations on the exploitation of the non-equilibrium character of the microwave plasma to promote the preferential excitation of the vibrational levels of CO_2 were however not successful[3–5,9,16]. The conditions under which high efficiency was achieved have not been reproduced to date. In recent experiments which closely follow the original design, up to 50 % energy efficiency was reported under conditions that point to a state close to local chemical equilibrium[13,41].

While the efficiencies of these sets of experiments and the proposed operating conditions vary significantly, the plasmas contraction dynamics as a function of pressure are very similar[45]. The optimal conditions for plasma conversion are found in the same pressure range of 100 mbar to 200 mbar[17,45], coinciding with a discharge mode transition. Despite these commonalities in the contraction behavior, the implications of the mode transitions on the plasma conditions remain largely unclear, since currently established theories of plasma contraction fail to describe the occurrence of these discharge modes.

A transition mechanism based on shifting non-equilibrium character of the discharge with increasing pressure is described by Fridman and Kennedy[16,17], initiated by VT-relaxation with increasing pressure and resulting in a shift from a vibrational non-equilibrium to quasi-equilibrium conditions[17]. Recent reports show that a VT-nonequilibrium can be ruled out for moderate pressure steady state conditions[13,41,45], which dismisses the non-equilibrium driven contraction mechanisms. Den Harder et al.[13] proposes a

pressure-induced transition as a result of a transitions from collisionless to collisional conditions. This mechanism relies on the wave propagation cut-off at the critical density n_c in low pressure conditions where the momentum transfer frequency of electrons with heavy particles (collision frequency ν_m) is below the angular driving frequency ω. Recently reported electron density measurements[45], however, show that both discharge modes are over-dense ($n_e > n_c$). This rules out a collisionality-induced contraction mechanism. Therefore we conclude that the contraction dynamics of the CO_2 microwave discharge has not been explained to a satisfactory degree. Particularly the effect of composition and associated changes in the thermodynamic properties of the plasma medium have not been considered in previous work.

The discharge contraction mechanisms are only well established for simple plasma systems in noble gases and nitrogen. The mechanisms of contraction have been described based on experimental[24,25] and modeling[19,28,34,36] efforts. For molecular gasses the two necessary conditions for contraction are non-uniform gas heating and the onset of molecular ion formation, which is followed by effective dissociative molecular ion recombination[31]. The non-uniform heating is driven mainly by the thermal-ionization instability, a mechanism that relies on positive feedback between an increase in temperature and stimulation of the ionization rate (via an increase of the reduced field (E/n) parameter)[28,31,35], resulting in a self-intensifying electron density growth. At low pressures, a dominance of ambipolar diffusion over volume recombination prevents contraction[14,28]. While these general mechanisms of contraction are also anticipated for more complex molecular discharges[34,36], they fail to address the influence of chemical reactions in reactive plasmas, particularly the consequences of significant thermally driven heavy-particle conversion and electronegativity[19].

Only recently the implications of chemical reactions on discharge mode instabilities were first described in a numerical study on reactive $H_2-O_2-N_2$ mixtures in a DC discharge[47]. The authors show by assessment of the coupling between plasma- and chemical kinetics, that the plasma thermal instability couples to a plasma chemical instability (PCI). The thermo-chemical heat exchange in the plasma, as a result of endothermic and exothermic reactions, is found to induce stability and instability, respectively, via the thermal-ionization mechanism. Also, plasma chemical instability is shown to be moderated by electron attachment processes. Both of these aspects are very relevant in CO_2 discharges. The thermal dissociation of CO_2, a highly endothermic process, and the shift in electronegativity in a partly decomposed CO_2 mixture as a result of the attachment to molecular oxygen, become important in CO_2 plasma with gas temperatures exceeding 2000 K[43]. Even so, while the reactive nature of the CO_2 microwave plasma likely influences the contraction dynamics significantly, this aspect has remained largely unexplored.

The main purpose of this paper is to formulate a consistent description of the observed discharge modes of the CO_2 microwave plasma in the range of 50 mbar to 1000 mbar. The plasma is characterized in terms of its geometric shape, gas temperature, and power den-

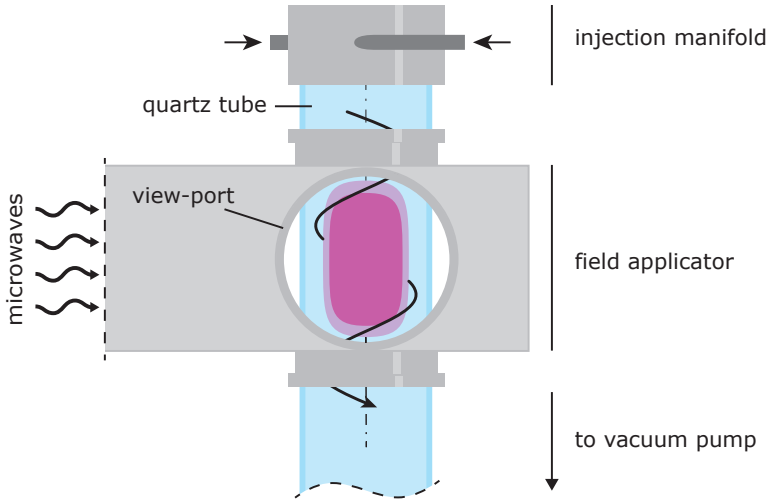

Figure 1: Illustration of the experimental setup, including the field applicator and the main plasma reactor components. The microwave source and impedance matching components are omitted. The view ports on either side of the waveguide provide optical access for the emission-based plasma diagnostics.

sity, obtained from optical emission profiles and the Doppler broadening thereof using the 777 nm O(^{5}S $\leftarrow$ ^{5}P) oxygen triplet emission. The evolution of these discharge parameters is interpreted in terms of the thermodynamic and dielectric properties of the discharge medium as a function of temperature. Two mechanisms are identified that explain the discharge modes; based on the coupling of the plasma-chemical instability and thermal instability, and resulting from the intricacies of plasma wave-coupling in high-frequency fields. The critical parameters for the onset of these mechanisms are identified, and its implications on the plasma parameters will be discussed. Furthermore, improved understanding of the instability and contraction mechanisms in reactive microwave plasmas are used to provide retrospective insight in the plasma conditions of previously reported CO_2 conversion experiments.

2 Experimental

The plasma is generated by 2.45 GHz microwaves using a WR340 waveguide-applicator configuration with vortex-stabilization. This plasma source configuration is extensively researched in context of gas processing applications [5,6,13,20,45].

An illustration of the field applicator configuration and discharge tube are shown in Fig. 1. The vacuum vessel consists of a quartz tube, 27 mm inner diameter and transparent for microwaves, and intersects the wide sides of the waveguide in the direction parallel to the TE_{10} field mode. Two nozzles are mounted tangentially in an injection manifold at the tube entrance in order to create a vortex flow. This stabilizes the plasma on the tube axis and provides gas-dynamic insulation of the plasma from the wall [21,45].

A waveguide short is fixed at a distance of a quarter wavelength from the tube axis. The standing wave created in this configuration has an anti-node that spatially coincides with the reactor tube, which is beneficial for plasma-wave coupling. An automatic 3-stub motorized impedance matching device (S-TEAM HOMER) provides both real-time impedance matching to the plasma conditions and power measurements. The incident (P_i) and reflected (P_r) power measurements have a specified error below 5 %. The power absorbed by the plasma $P_\mathrm{abs} = P_\mathrm{i} - P_\mathrm{r}$, assuming there are no losses to the environment. A coupling efficiency $(P_\mathrm{i} - P_\mathrm{r})/P_\mathrm{i}$ exceeding 99.9 % is achieved under a wide range of operating conditions. Under matched conditions the reflected power can therefore be neglected. Two view ports mounted in the short sides of the waveguide on opposite sides of the quartz tube provide optical access for the optical diagnostics, which are used to measure the gas temperature measurements and the plasma emission intensity profile.

The geometric dimensions of the discharge are obtained from the full-width at half intensity of the 777 nm oxygen triplet emission using the same approach as described in Wolf (2019) [45]. A narrow spectral band-pass filter is used to isolate these emission lines and recorded with a CCD sensor. Radially resolved intensity profiles are obtained by applying a discrete inverse Abel transform using the Hansen and Law method [22].

The relation between the 777 nm emission intensity $\mathcal{I}_{777}$ and electron density n_e can be described in good approximation by [45]:

$$\mathcal{I}_{777}(r,z) \propto n_e(r,z) \tag{1}$$

since it is driven mostly by electron impact excitation, and scales with the population rate of the upper state upper state $n_e n_O k_{ee}$. Here n_O is the ground state atomic oxygen density and k_{ee} is the rate constant of electron impact excitation of the transition. Both the reduced field (E/n) and gas temperature T_gas are found to have only weak axial and radial dependency in comparison to the electron density profile in our experimental conditions. Furthermore we have assumed in Eq. 1 that the O production is dominated by heavy-particle reactions over electron-impact reaction, which is likely at gas temperatures values above 3000 K. While this assumption is expected to break down only at lower gas temperature values ($p < 100$ mbar), the resulting error in the plasma size values remains limited to a factor $\sqrt{2}$ in the extreme case where all oxygen production is driven by electron-induced processes [45].

The power transferred from the electric field to the plasma electrons is described by Joule heating. For an oscillating field with radial frequency ω, a peak field amplitude E_0, and electron conductivity σ, the power density is described by [31]:

$$\mathcal{P}_\Omega = \frac{\sigma E_0^2}{2} = \frac{E_0^2}{2}\frac{e^2}{m_\mathrm{e}\nu_\mathrm{m}}\frac{\nu_\mathrm{m}^2}{\nu_\mathrm{m}^2+\omega^2}n_e \tag{2}$$

Here ν_m and n_e represent the electron-neutral mean collision frequency for momentum

transfer (collision frequency) and the electron density respectively. Both E_0 and ν_m are assumed constant over the plasma, which is supported by simulations of the field coupling to the microwaves for plasma conditions presently studied [20]. By substituting Eq. (1) into Eq. (2) and normalization of the spatially integrated power density to the total absorbed power, an explicit expression of the spatially resolved power density is obtained.

$$\mathcal{P}_\Omega(r,z) = \frac{P_\mathrm{abs}}{2\pi \iint_{r,z} \mathcal{I}(r,z) r\, dr\, dz} \mathcal{I}(r,z), \tag{3}$$

Gas temperature measurements in the plasma are obtained from the Doppler broadening of the 777 nm oxygen triplet lines, analogous to Ref. [45]. The three emission peaks are resolved and the Doppler broadening is taken from the Gaussian component. The pressure broadening mechanisms is in good approximation Lorentzian. Only Van der Waals broadening is significant under the present operating conditions. A rough estimate obtained with the impact approximation, following Kunze (2009) [26], indicates a Lorentzian component of around 1 pm, which is small compared to the Doppler broadening and in good agreement with experimentally observed values in the full measurement range.

The measurements are spatially resolved in the lateral direction by projection on a linear optical fiber array. The axial coordinate is scanned using a translation stage. The collected light is dispersed using a Littrow-configuration spectrometer (2^nd order of a 1180 lines/mm grating, $f = 2.25$ m, slit diameter: 50 µm) and detected using a CCD camera. The low emission intensity of the low pressure plasma conditions required an averaging over three 60 s exposures to keep the fitting errors below 5 % of the measured value. An important implication of this time-averaged measurement is that temperature values can only be obtained for steady-state plasma conditions.

3 Results

Three fundamental discharge modes are identified in the CO_2 microwave plasma between 50 mbar and atmospheric pressure. The visual appearance of the modes, including also a hybrid regime, are shown in Fig. 2. In previous publications [13,16,17,20], discharges (i) and (ii) are commonly referred to as the *diffuse mode*, and discharges (iii) and (iv) as the *contracted mode*. Since the mode classification described in this paper expands on the these definitions, we adhere to a new nomenclature. From low to high pressure (left to right in Fig. 2) the discharge modes are referred to as (i) the *homogeneous mode*, (ii) a *low confinement mode* (L-mode) and (iv) a *high confinement mode* (H-mode). The hybrid discharge state (iii) shows simultaneous features of both the L-mode and H-mode plasmas.

- In the *homogeneous mode* the discharge emission exhibits a homogeneous appear-

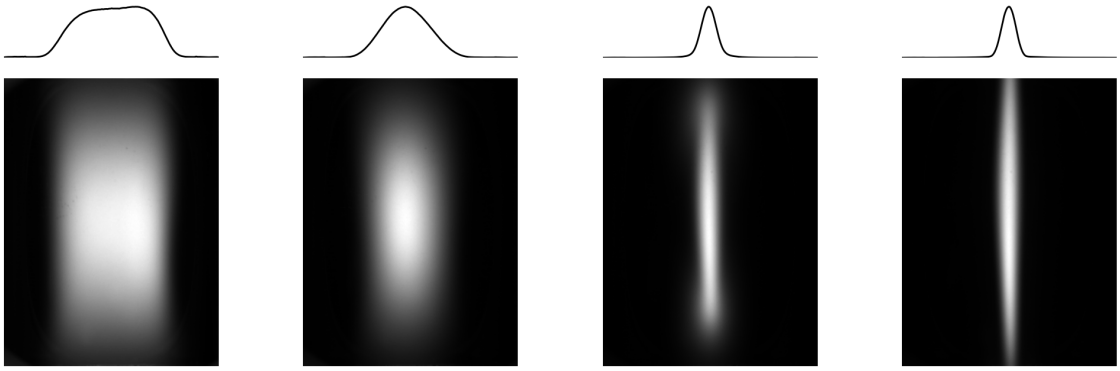

(i) homogeneous (ii) L-mode (iii) hybrid (iv) H-mode

Figure 2: Photos of 4 characteristic states of the vortex-stabilized CO_2 microwave plasma with increasing pressure from left to right. The associated lateral emission intensity profiles are displayed above. The intensity is normalized in each image to maximize contrast.

ance, with a luminous intensity that is constant over the discharge (Fig. 2(i)). This mode is visually distinguished from the others by a relatively flat lateral luminosity, which indicates a flat or even hollow radial emission intensity profile. While the discharge tends to expand to the full volume of the discharge tube, the plasma is axially contained by the extent of the waveguide and radially by the vortex flow.

- The *low confinement mode (L-mode)* contracts in both the axial and radial direction with respect to the homogeneous discharge mode. The lateral emission is characterized by a Gaussian profile (Fig. 2(ii)). The filament diameter varies between 10 mm to 20 mm depending on the power and pressure, which is related to the local skin depth[45].

- The *high-confinement mode (H-mode)* has the appearance of a narrow elongated filament with a radius of 2 mm to 4 mm, spanning the entire waveguide height (Fig. 2(iv)). The discharge radius remains skin depth limited, which is found to scale with input power but is independent of pressure[45]. Apart from radial contraction, axial elongation of the discharge column is another distinctive characteristic of the H-mode plasma.

- The *hybrid regime* is a transition state in which the plasma filament simultaneously exhibits features of both L- and H-mode plasmas along the axial discharge coordinate (Fig. 2(iii)). As the pressure increases, the onset of the H-mode occurs first in the center of the filament and grows outwards towards the tips.

Power density profiles in Fig. 3 are obtained from plasma emission profiles at a fixed power input of 860 W using Eq. (3). The progressive states of discharge contraction with rising pressure are more clearly visualized in this manner.

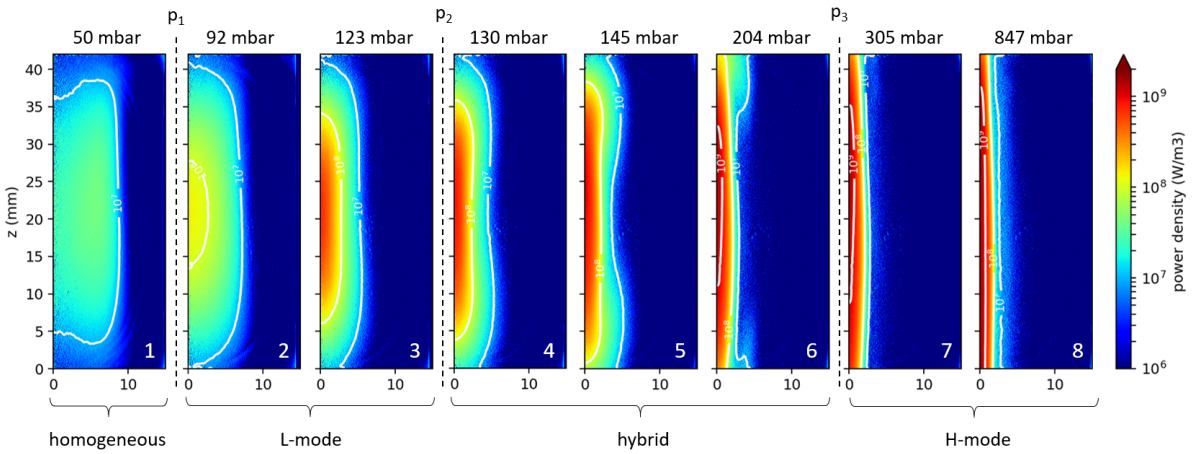

Figure 3: Power density profiles of a microwave discharge in CO_2 as a function of pressure, with an input power of 860 W. The distinct discharge regimes are indicated below.

The evolution of plasma dimensions, power density and the gas temperature in the center of the plasma are provided in Fig. 4. The mode transitions are marked by abrupt changes in the radial and axial dimensions of the filament, as indicated in Fig. 4(a-b). The threshold pressures of transitions between the discharge modes for a fixed power input depend mostly on pressure. In general, an increase of input power results in a decrease in the pressures where the transitions occur. The flow rate is found to weakly influence the discharge parameters, which is in line with previous observations on flow dependence of gas temperature, geometry and electron density[39,45]. Therefore the gas flow is not further considered in the remainder of this paper. As will be shown later, the decoupling of the plasma processes and flow dynamics enables treating the plasma as a heat source by means of the power density.

The elongation observed in the H-mode are likely a result of surface waves formation, considering its resemblance to surface-wave induced elongation in surface-wave sustained microwave discharges[15]. Surfatron and Surfa-guide reactors plasma columns are known to extend far beyond the boundaries of field applicator[32]. Since the plasma must be sufficiently collisional ($\nu_c > \omega$) and conductive to effectively couple the fundamental TE_{10} wave-guide mode to the surface waves[30], the strong increase of the ionization degree observed in the transition from L-mode and H-mode conditions[45] may explain the observed elongation observed at the onset of the H-mode. A simultaneous rise in microwave radiation observed outside of the applicator at this, particularly in conditions of higher power and pressure, indicate leakage of power to the environment induced by coaxial coupling of the TE_{10} field mode. An important implication of elongation and the resulting coupling losses associated with the H-mode discharge is that a highest overall state of discharge confinement is reached under hybrid plasma conditions, where the filament is both radially contracted and axially contained. The peak temperature values in the hybrid conditions around p_2 to p_3 may be explained by the optimal state of contraction and coupling efficiency in this regime. We note that the later may lead

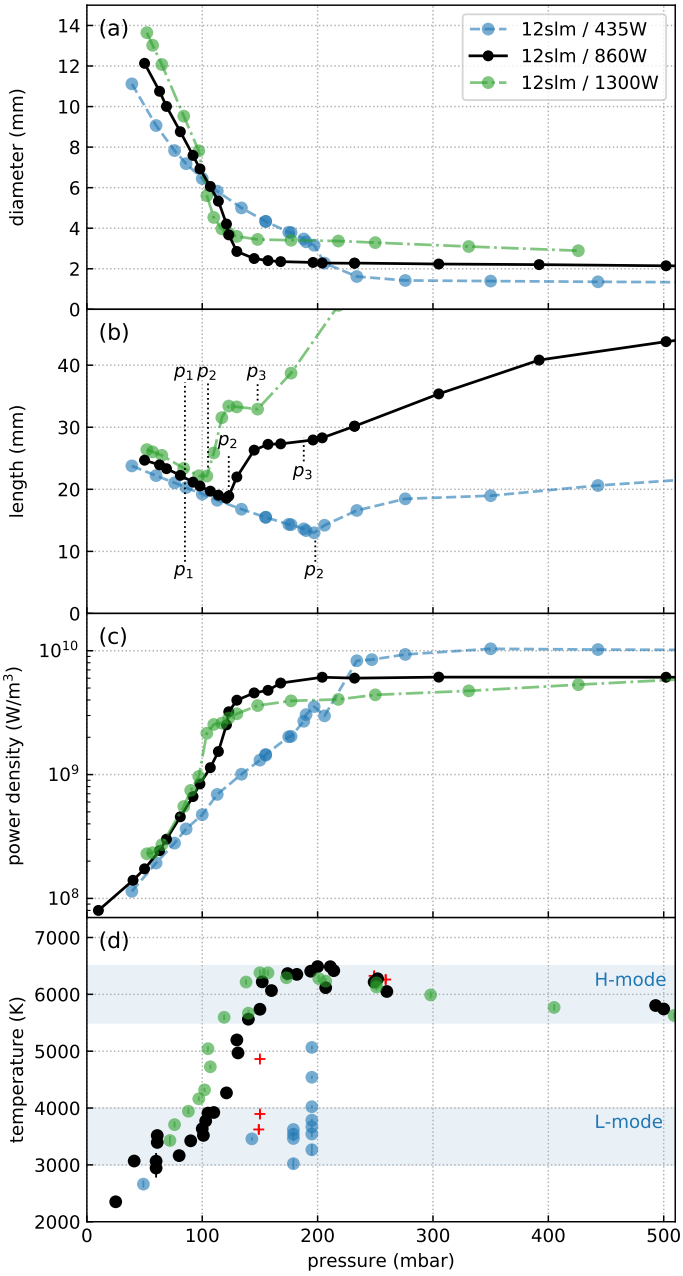

Figure 4: Evolution of plasma parameters for rising pressure, including the diameter (a) and length (b) of the plasma filament, the average power density (c) and the gas temperature (d)

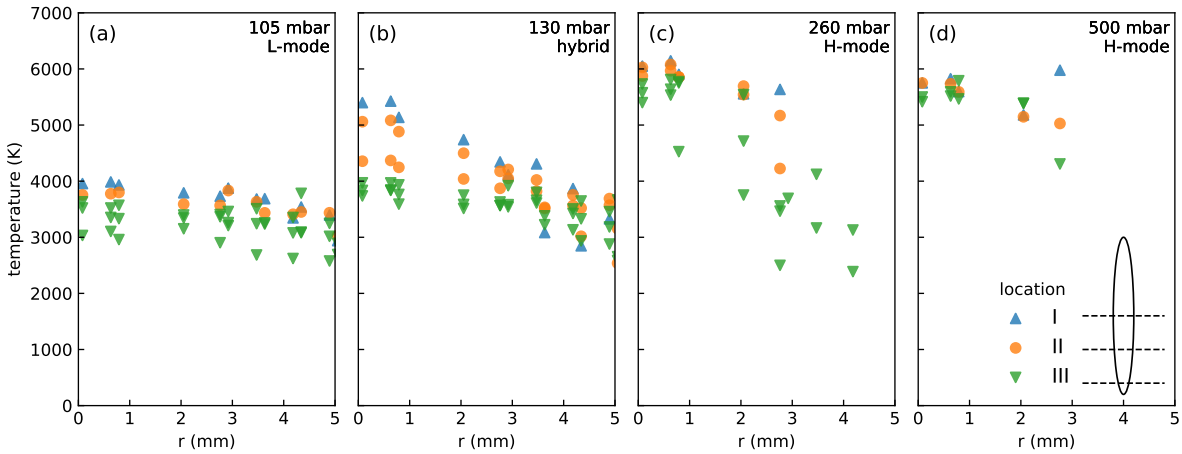

Figure 5: Lateral temperature profiles for L-mode, H-mode and hybrid conditions, obtained in plasmas at the specified pressures and an input power of 860 W. The temperature cross sections are obtained at locations in the center of the waveguide (I), at the edge (III), and halfway (II)

an power leakage at high pressure, which in the exrtreme case of atmospheric conditions constitutes an estimated 10% of the input power. This effect not presently accounted for in the power density values in Fig. 4(c). Other causes of the temperature reduction with rising pressure may also include changes in the heat transfer mechanisms or macroscopic gas-dynamic flow patterns.

The gas temperature measurements presented in Fig. 4(d) show that the H-mode and L-mode conditions are associated with distinct gas temperature ranges. The L-mode plasma has a gas temperature of approximately 3500 K to 4000 K, while the H-mode conditions occur at a temperature of 5500 K to 6500 K, as illustrated by the shaded regions. The distinction in temperature between the modes is most evident at low values of P_{abs} as a result of the considerably higher transition pressure. The plasma remains below 4000 K up to the transition pressure of 200 mbar, after which a sharp in crease in temperature is observed.

The distinct H-mode and L-mode gas temperatures in the center of the discharge also extend throughout the discharge. The spatially resolved temperature profile measurements shown in Fig. 5(a) and (d) show flat spatial temperature distributions for both L-mode (3000 K to 4000 K) and H-mode (5500 K to 6500 K) plasmas. The temperature distribution of the intermediate hybrid conditions (Fig. 5(b)) shows radial temperature profiles associated with the H-mode in the central region of the filament (z = 19 mm to 25 mm), while the temperature profiles in the edges show an L-mode temperature profile. The co-existence of both L-mode and H-mode conditions along the axis of the filament hybrid mode may be explained by spatial variations in the applied field strength caused by view ports and access ports for the quartz tube in the waveguide. Note that the lowest power input in the confined regime leads to the highest power density, which is probably related to field enhancements associated with plasma impedance changes under matched

conditions.

In conclusion, the distinct temperature ranges observed for L-mode and H-mode discharges demonstrate that the governing mechanisms are closely related to the gas temperature. Power and pressure, on the other hand, do not directly influence the temperature of the discharge modes, and rather function as independent control parameters by determining which mode comes to expression (Fig. 8).

From Fig. 3 and Fig. 4(d) we observe that the power density has a non-linear relationship with respect to the gas temperature. In the L-mode, the power density increases exponentially by an order of magnitude with rising pressure, while the gas temperature only increases by a third, from roughly 3000 K to 4000 K. To put these observations in perspective, we will now discuss the properties of CO_2 under chemical equilibrium conditions. To do this, we first calculate the thermodynamic equilibrium properties of CO_2 for the temperature range observed in the experiments, i.e. composition and the specific heat capacity of the reactive system. As a starting point, the enthalpy of the equilibrium mixture is calculated under assumption of ideal mixing,

$$h_{\mathrm{mix}} = \sum x_i H_i \tag{4}$$

where H_i is the enthalpy of each species i in the mixture with mole fractions x_i. The thermodynamic coefficients for the dominant neutral species (e.g. CO_2, CO, O_2, O and C) are obtained from the NASA Glenn library [29] for a temperature range of 200 K to 20 000 K. Ions and electrons are not considered in the calculations, since the plasma has a low ionization degree (10^{-4}) and a gas temperature below 6500 K which is well below the first ionization threshold of CO_2 at 15 000 K [46]. Although plasma-driven processes such as electronic excitation are known to influence the thermodynamic properties [7,8] under LTE conditions (where $T_e = T_{\mathrm{vib}} = T_{\mathrm{rot}} = T_{\mathrm{trans}}$), such contributions can be neglected un first approximation based on the assumption that the heavy particle kinetics dominate over the electron-induced chemistry. This is warranted since the plasma deviates from chemical equilibrium, with T_e 1-2 eV and is only weakly ionized.

Following the procedure detailed in Ref. [45], x_i of the equilibrium state are calculated by minimization of the Gibbs free energy for given pressure and temperature. The specific heat capacity c_p is defined for a fixed pressure as

$$c_p = \left.\frac{\partial h_{\mathrm{mix}}}{\partial T}\right|_p, \tag{5}$$

which includes both the heat capacity of the gas species associated with the internal and translational degrees of freedom (frozen), and a reactive component which involves the heat of formation required to bring the mixture to a state of local thermodynamic equilibrium composition at a given temperature T. The specific energy input in thermodynamic equilibrium, $q_{\mathrm{te}}(p,T)$, required per initial CO_2 molecule to reach a state of

thermodynamic equilibrium by isobaric heating trajectory from T_0 to T_{gas} is obtained by integration over c_p.

$$q_{\mathrm{te}} = \frac{M_{\mathrm{CO_2}}}{eN_A} \int_{T_0}^{T_{\mathrm{gas}}} c_p(T) dT \tag{6}$$

Here $M_{\mathrm{CO_2}}$ is the molar mass of CO_2, N_{A} is Avogadro's constant and e is the elementary charge. Figure 6a shows the calculated thermodynamic equilibrium properties of the heated gas at pressures of 10 mbar, 100 mbar and 1000 mbar. Both the composition and specific heat capacity of the thermodynamic equilibrium mixture are very much temperature-dependent, which is a results of the distinct thermal dissociation thresholds associated with each molecular species in the mixture. Above 2000 K the CO_2 mixture progressively decomposes with rising temperature, producing increasingly smaller molecules. Between 3000 K to 4000 K the mixture is dominantly composed of CO, O_2 and O. Above 7000 K to 8000 K the mixture becomes mono-atomic, composed of mostly O and C. As the gas pressure increases, the thresholds of thermal dissociation shift to higher temperatures in agreement with Le Chatelier's principle[40].

Figure 6b shows that the total specific heat capacity (frozen + reactive component) for CO_2 is largely determined by the reactive contribution. The calculated values correspond reasonably well to literature values[40,46], both in terms of the absolute values and the peak occurrence. The two peaks in the specific heat around 3000 K and 6000 K correspond to the thermal dissociation thresholds of CO_2 and CO, respectively[46]. The difference between the frozen and reactive contributions to the specific heat capacity represents the energy invested in the dissociation of molecular species. The evolution of the temperature in response to the specific energy input q_{te} is calculated using Eq. (6) and shown in Fig. 6c. The span in specific energy input associated with these stable temperature regions corresponds to the bond-energies of the CO−O bond (5.51 eV) and C−O bond (11.16 eV).

The gas temperature, associated with the L-mode and H-mode plasma conditions, coincides with regions of high c_p, as indicated in Fig. 6. It therefore appears that the observed temperature plateaus around 3000 K and 6000 K correspond to the dissociation thresholds for CO_2 and CO, respectively. This notion is corroborated by the plateaus that emerge in the relation between the gas temperature and the power density in Fig. 7. Thermodynamic regions of high reactive heat capacity result in a weak correlation power density and gas temperature. This suggests that the plasma medium is c_p-controlled and in a state close to chemical equilibrium with the gas temperature. The commonly observed peak temperature values of 6000 K to 7000 K in moderate to high pressure CO_2 microwave plasmas[5,13,45] and plasma CO_2 torches[10,27,39] fit in this interpretation. This apparent temperature barrier around 6000 K to 7000 K follows from the large energy input (from 10 eV to over 20 eV per molecule according to Fig. 6c) required to bridge this temperature range including equilibrium reactions.

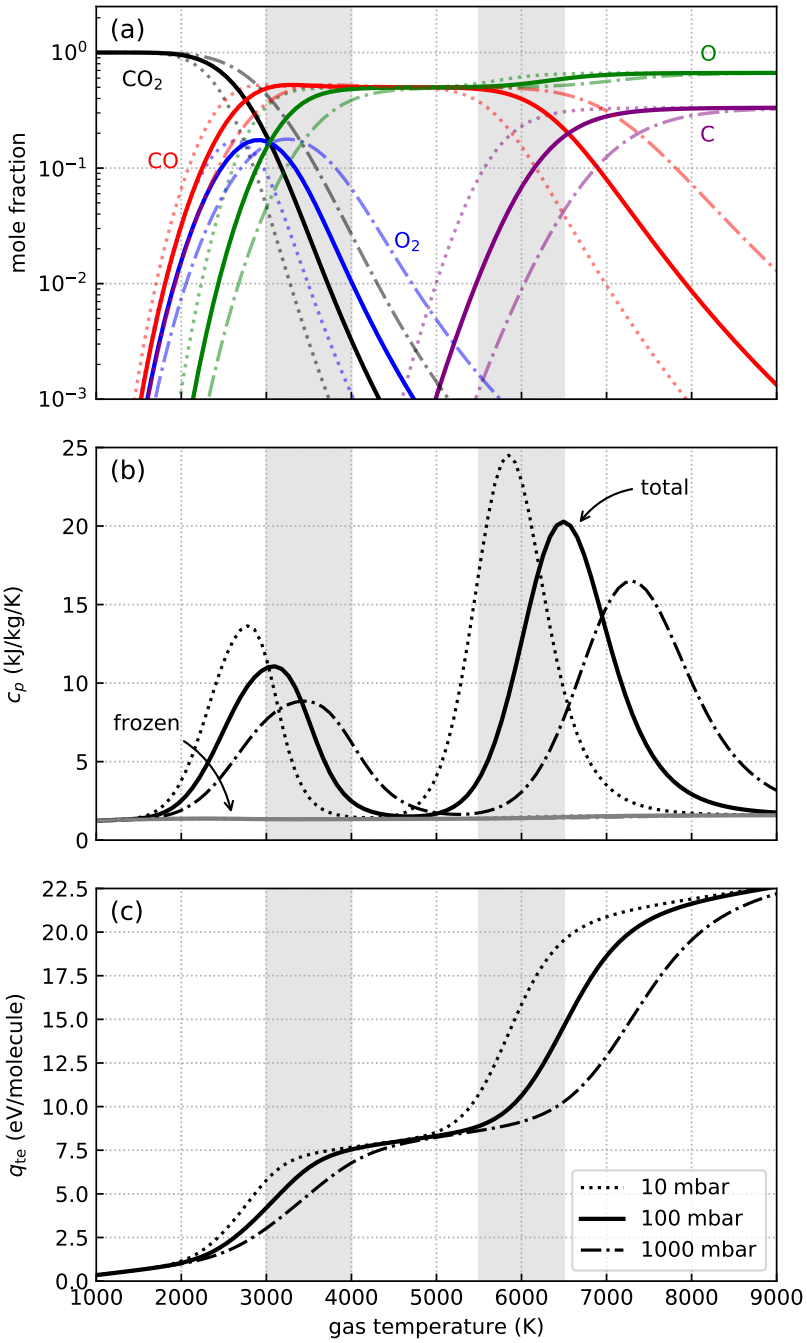

Figure 6: Calculations of the thermodynamic equilibrium properties of CO_2 as a function of temperature at fixed pressure. a) thermodynamic equilibrium composition, b) specific heat capacity including equilibrium reactions (total) and excluding equilibrium reactions (frozen), c) specific energy input per molecule of reactant CO_2 in relation to the mixture temperature, relative to 300 K. The shaded areas indicate the experimentally observed L-mode and H-mode temperature regimes.

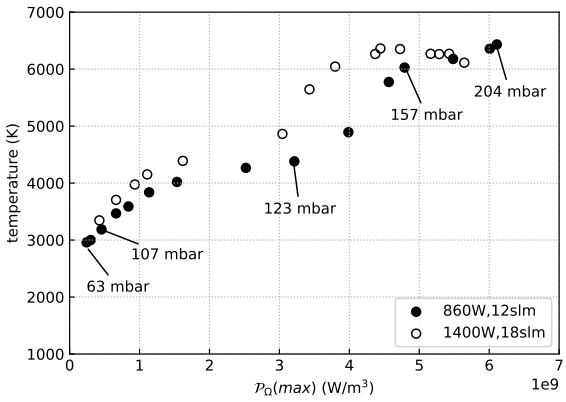

Figure 7: Peak power density $\mathcal{P}_\Omega$ in the discharge in relation to the gas temperature in the center of the plasma.

4 Discussion

The characterization of discharge in the previous section lays the foundation for a classification of the discharge modes. Two governing mechanisms are proposed, which rely on the interplay between collisionality ν_c/ω and wave absorption, and the thermodynamic properties of the plasma medium as a result of its reactive nature. An overview of the subatmospheric modes of CO_2 microwave plasma are illustrated in Fig. 8. The transition pressures (p_1 to p_3) define the parameter space of the discharge in terms of pressure and power, as illustrated in the lower panel in Fig. 8.

The homogeneous discharge mode results from a cut-off in the plasma wave dispersion properties at low pressure. The wave-propagation cut-off imposes a limit on the electron density to its critical value n_c when the collisionality is low in relation to the driving frequency ($\nu_\mathrm{m}/\omega < 1$)[2,13,23,31], where ν_m is the momentum transfer frequency of the electrons with heavy particles, ω is the driving frequency and $n_\mathrm{c} = \epsilon_0 m_\mathrm{e}\omega^2/e^2$ is the frequency dependent critical density. Since the imaginary value of the wave-number becomes purely imaginary in a low-collisional super-critical ($n_e > n_\mathrm{c}$), the dispersion cut-off leads to reflection of microwaves at the over-dense plasma boundary. This inhibits further electron density growth and effectively imposes under-dense conditions ($n_e < n_\mathrm{c}$) in the center of the plasma as long as ($\nu_\mathrm{m}/\omega < 1$). In some cases this may even lead to hollow profiles. For a driving frequency of $\omega = 2.45\,\mathrm{GHz}$ the electron density is limited to $n_\mathrm{c} = 6 \times 10^{17}\,\mathrm{m}^{-3}$ in low-pressure conditions.

The collision frequency calculations for homogeneous mode conditions (T_gas =3000 K to 4000 K, $n_e = n_\mathrm{c} = 7 \cdot 10^{18}\,\mathrm{m}^{-3}$, $T_e = 1\,\mathrm{eV}$ to $2\,\mathrm{eV}$) shows that $\nu_\mathrm{m} < \omega$ in this regime, with calculations following the approach by Wolf (2019)[45]. The transition criterion ($\nu_\mathrm{m} = \omega$) predicts a critical pressure between 60 mbar to 90 mbar, which is in line with the experimentally observed value of approximately 85 mbar. The critical pressure is almost constant with rising input power. This behavior is a characteristic of the critical density limited regime, resulting from the limit the latter imposes on the power density

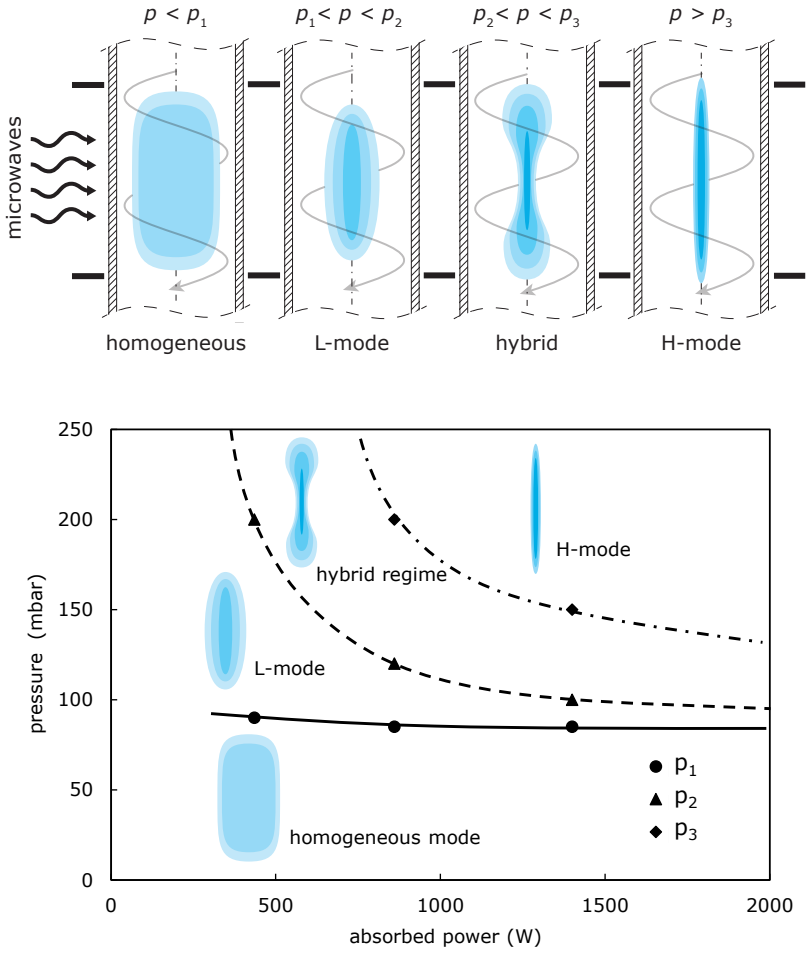

Figure 8: Top: Illustration of the distinct regimes in the subatmospheric CO_2 microwave plasma. Bottom: Schematic of the parameter space, indicating the occurrence of the discharge modes. The transition boundaries are freely extrapolated from the transition pressures determined from Fig. 4

(which scales with n_e according to Eq. 2) with rising input power. The observed $\mathcal{P}_\Omega$ values in Fig. 4 indeed remains constant with rising power, consequently leading to fixed temperature and collisionality values, and ultimately a critical pressure which does not depend on P_{abs}.

While the electron density of the homogeneous mode regime has not been directly measured, the spatial extent of the plasma indicates that the electron density is around its critical density of $6 \times 10^{17}\,\mathrm{m}^{-3}$. The skin-depth in the under-dense regime ($\delta = c/\omega_{\mathrm{pe}}$) is approximately 2 cm at the critical density. The radial plasma dimensions, as observed from the emission profiles in Fig. 4a, remain below this skin-depth value. This shows that the plasma is not skin-depth limited in this regime. The absence of contraction in the homogeneous mode appears to be a directly related to the associated electron density limit. The discharge contraction phenomenon relies heavily on self-intensifying electron density growth[28,31,35] such as the thermal-ionization instability. It appears that the electron density limit imposed by the wave-dispersion cutoff suppresses the contraction in high frequency discharges in the homogeneous regime. This this implies that the cut-off behavior which applies in low-collisional AC plasmas suppresses the thermal-ionization contraction instability, even at elevated pressures, until collisional wave absorption sets off.

The mechanism that governs the L-mode to H-mode transition instability differs fundamentally from the critical-density moderated thermal-ionization instability mechanism described above. In contrast to the homogeneous mode, both L-mode and H-mode plasmas are in a collisional, contracted state[45]. A correlation is found between the stability of the discharge in the two contracted modes and the enhanced heat capacity of the reactive gas mixture (c.f. Fig. 6(c)) at their respective gas temperatures. This observation can be explained by a coupling between the plasma-chemical balance and the thermal instability via thermal-ionization mechanism, as proposed by Zhong (2019)[47] for plasmas in reactive gas flows. The specific heat increase of the reactive plasma as a function of temperature results in a weak temperature response and moderation of thermal-ionization contraction instability, resulting in a thermal stability of the plasma. Conversely, the unstable nature of the transition between the L-mode and H-mode, characterized by a low reactive specific heat and a rapid increase in gas temperature with a small perturbations in input conditions, enhance the thermal-ionization instability. This thermo-chemical c_{p}-*controlled stability* corroborates the previously proposed stabilizing effect of endothermic reactions on reactive plasmas[47], as the stable plasma conditions in both the L-mode and H-mode appear to be a consequence of the strongly endothermic nature of the CO_2 dissociation process. Table 1 provides a summary of governing mechanisms and typical parameters associated with each mode.

This c_{p}-controlled stability mechanism predicts a number of distinct contracted discharge modes equal to the distinctly separated dissociation and ionization thresholds of the working gas. In the case of CO_2, the large separation of the bond energies of CO_2

Table 1: Overview of discharge parameters and mechanisms associated with the distinct discharge modes

	homogeneous	L-mode	H-mode
appearance	diffuse	contracted	contracted
pressure thresholds	$<p_1$	$p_1 < p < p_2$	$>p_3$
gas temperature	<3000	3000-4000	5500-6500
stabilization mechanism	n_e cut-off limit	c_p-controlled	c_p-controlled
ν_m/ω [45]	< 1	$1-2$	$1-10$
n_e/n_c [45]	$\leqslant 1$	$10-100$	$100-1000$

(5.51eV) and O_2 (5.15eV) and the much higher bond energy of CO (11.2eV) lead to the two contracted discharge regimes. In comparison, N_2 only has a single dissociation threshold at approximately 7000 K [12], which seems to agree with temperature measurements of 7000 K reported in N_2 microwave plasmas at a pressure of 800 mbar [18].

The chemical equilibrium calculations underlying the preceding analysis provide valuable insight into the nature of the discharge modes and the governing mechanisms, despite disregarding the potential effects of electron-driven kinetic processes. However, processes such as electron impact dissociation, dissociative recombination and attachment may incur composition changes that lead to deviations from chemical equilibrium, and subsequently, lead to complicated kinetic effects on plasma-instability [19,47]. A rise in oxygen concentration, for instance, may enhancement of attachment reactions, which may both stabilize the thermal instability by suppressing the electron density growth, while simultaneously enhancing destabilizing oxidation processes via exothermic heat release [47]. Such complicated dynamics are also anticipated in CO_2 plasmas since heated CO_2 in chemical equilibrium is known to acts as an electronegative gas at 3000 K and becomes recombination-dominated above 5000 K [43]. This suggests that the H-mode and L-mode plasmas are governed by distinct charged particle kinetics. In the temperature regime of the L-mode, the electron balance is likely influenced significantly by electron attachment due to the presence of O_2. This pathway is lost in the H-mode conditions as a result of the low O_2 concentrations at the associated gas temperatures. The constant ionization degree and plasma diameter as a function of the pressure for a fixed power in the H-mode indicates a dissociative-recombination controlled charged particle balance [45], with the dominant molecular ion (e.g. CO^+). The dominant charged particle kinetics in relation to the contraction dynamics in complex reactive plasmas such as CO_2 is however still not fully understood. This asks for detailed plasma-kinetic modeling where both the effect of plasma processes and gas dynamics on the composition should be considered.

Now that the basic mechanisms underlying of the moderate to atmospheric pressure discharge modes in CO_2 has been established, the implications of the discharge parameters on the performance of plasma-induced CO_2 conversion can now be discussed. We have previously proposed that the optimal discharge pressure in terms of energy efficiency,

commonly reported between 100 mbar to 200 mbar for microwave CO_2 discharges[13,16,17], is related to the L-mode to H-mode transition[45]. The similarities in contraction dynamics identified in the same study, between the recent reported on high temperature conversion and the original high efficiency results, show that the plasma temperature in Ref.[6] was likely similar. This suggests that the contribution of thermally driven conversion in the highly efficient plasma conditions that yielded 70-80 % energy efficiency was much more significant than initially recognized. The high gas temperature inherently linked to the H-mode and L-mode of CO_2 rules out the non-equilibrium interpretation that relies on low translational temperatures to drive vibrational excitation and dissociation via the Treanor effect.

The present work shows that the contracted discharge modes emerge as a property of the reactive plasma, governed by the distinct dissociation thresholds of the molecular species. Therefore, the prevailing non-equilibrium plasma interpretation used to explain the favorable plasma conditions around 100 mbar to 200 mbar[1,6,16,17,37] is unlikely, given the importance of thermally driven chemical reactions on these types of discharge modes. The favorable conditions for efficient plasma-driven conversion in CO_2 in the 100 mbar to 200 mbar range can be explained by a shift in the dominant thermal heavy particle kinetics in the discharge. The L-mode plasma conditions lead to increased CO production with rising pressure, while the rising selectivity to atomic carbon in H-mode plasmas and the increase in subsequent recombination pathways in the discharge afterglow lead to diminishing returns. More generally, the reduction in the energy efficiency observed for increasing pressure may also be attributed to the enhancement of 3-body association reactions, (O + O + M) and (O + CO + M) or the coaxial field losses observed at high operating pressures.

The thermodynamic energy efficiency limit of around 50% for thermal conversion[13], calculated in a closed system where all oxygen radicals associate to O_2, agrees well with the energy efficiency values up to 50% reported for recent experiments. An advanced super-ideal quenching scenario is described in which the efficient O + CO2 reactions are promoted over oxygen recombination[16]. In this manner, by optimization of the cooling trajectory of the plasma products, a thermal dissociation process efficiency of over 70% is achievable[16,41]. This underlines the potential of thermal conversion and the importance of the cooling trajectory therein in optimizing the energy efficiency in CO_2 microwave plasmas. Efforts to understand and improve the overall plasma conversion performance, therefore, require careful optimization of the dissociation process in and around the plasma in conjunction with the subsequent cooling trajectory.

5 Conclusion

This work presents a first systematic experimental investigation into the nature of the discharge modes of CO_2 microwave plasmas in subatmospheric conditions. The contrac-

tion dynamics and the final stable contracted states have been investigated, providing insights into the discharge modes, the underlying mechanisms of formation, and their critical parameters of onset.

A homogeneous mode and two contracted modes have been identified between 50 mbar and atmospheric pressure. The homogeneous conditions are explained by a critical-density limit, imposed by the cut-off frequency of wave propagation, and suppressing the discharge contraction until a pressure where collisional conditions are reached. Multiple contracted modes are found to arise under conditions of high reactive heat capacity, governed by a thermo-chemical instability that arises from the coupling of the thermal-ionization instability and the thermally driven chemical conversion in the plasma. For CO_2 plasma, the endothermic nature of the thermally driven CO_2 and CO dissociation reactions are found to lead to the stable operating conditions of the L-mode and H-mode, respectively. The difference in the appearance of these contracted modes results from the evolution of charged particle kinetics in response to the shifting chemical composition. Modeling with detailed chemical kinetics is required to quantify the observed contraction dynamics.

We hope that the mechanisms of plasma instability and discharge mode formation described in this work will aid in the understanding and further development of technological plasmas for plasma-chemical applications. Specifically, the nature of the CO_2 contraction dynamics shows that previously reported results on highly efficient microwave driven plasma conversion of CO_2 likely rely on thermal conversion as the primary dissociation mechanism. Optimization of the CO_2 conversion process in microwave plasmas, therefore, asks for an approach where the plasma conditions are optimized for thermal conversion in conjunction with the cooling trajectory of the plasma products.

6 Acknowledgment

This research has been carried out as part of the Plasma Power to Gas research program with reference 13581, which is co-financed by the Netherlands Organization for Scientific Research (NWO) and Alliander N.V.

References

[1] R. Asisov, A. Fridman, V. Givotov, E. Krasheninnikov, B. Patrushev, B. Potapkin, V. Rusanov, and M. Krotov. Carbon dioxide dissociation in non-equilibrim plasma. In *Proc. 5th Intern. Symp. Plasma Chemistry*, volume 2, page 774, 1981.

[2] D. Attwood. Microwave scattering from an overdense turbulent plasma. *Physics of Fluids*, 17(6):1224–1231, 1974.

[3] I. Belov, V. Vermeiren, S. Paulussen, and A. Bogaerts. Carbon dioxide dissociation

in a microwave plasma reactor operating in a wide pressure range and different gas inlet configurations. *Journal of CO2 Utilization*, 24:386–397, 2018.

[4] A. Berthelot and A. Bogaerts. Modeling of CO 2 Splitting in a Microwave Plasma: How to Improve the Conversion and Energy Efficiency. *The Journal of Physical Chemistry C*, 121(15):8236–8251, apr 2017.

[5] W. A. Bongers, H. Bouwmeester, A. J. Wolf, F. P. J. Peeters, S. Welzel, D. van den Bekerom, N. den Harder, A. Goede, M. Graswinckel, P. W. Groen, J. Kopecki, M. Leins, G. van Rooij, A. Schulz, M. Walker, and R. van de Sanden. Plasma-driven dissociation of CO 2 for fuel synthesis. *Plasma Processes and Polymers*, 14(6):1600126, jun 2016.

[6] Y. Butylkin, V. Zhivotov, E. Krasheninnikov, M. Krotov, V. Rusanov, Y. Tarasov, and A. Fridman. Dissociation of CO2 by a plasma-chemical process in a nonequilibrium microwave discharge. *Sov. Phys. Tech. Phys.*, 26(5):555, 1981.

[7] M. Capitelli, D. Bruno, G. Colonna, C. Catalfamo, and A. Laricchiuta. Thermodynamics and transport properties of thermal plasmas: The role of electronic excitation. *Journal of Physics D: Applied Physics*, 42(19), 2009.

[8] M. Capitelli, R. Celiberto, G. Colonna, F. Esposito, C. Gorse, K. Hassouni, A. Laricchiuta, and S. Longo. *Fundamental Aspects of Plasma Chemical Physics*, volume 85. 2016.

[9] G. Chen, T. Godfroid, N. Britun, V. Georgieva, M. P. Delplancke-Ogletree, and R. Snyders. Plasma-catalytic conversion of CO2 and CO2/H2O in a surface-wave sustained microwave discharge. *Applied Catalysis B: Environmental*, 214:114–125, 2017.

[10] S. Chun, D. Shin, S. Ma, G. Yang, and Y. Hong. CO2 Microwave Plasma—Catalytic Reactor for Efficient Reforming of Methane to Syngas. *Catalysts*, 9(3):292, 2019.

[11] W. C. Chung and M. B. Chang. Review of catalysis and plasma performance on dry reforming of CH4 and possible synergistic effects. *Renewable and Sustainable Energy Reviews*, 62:13–31, 2016.

[12] V. Colombo, E. Ghedini, and P. Sanibondi. Thermodynamic and transport properties in non-equilibrium argon, oxygen and nitrogen thermal plasmas. *Progress in Nuclear Energy*, 50(8):921–933, 2008.

[13] N. den Harder, D. C. M. van den Bekerom, R. S. Al, M. F. Graswinckel, J. M. Palomares, F. J. J. Peeters, S. Ponduri, T. Minea, W. A. Bongers, M. C. M. van de Sanden, and G. J. van Rooij. Homogeneous CO 2 conversion by microwave plasma: Wave propagation and diagnostics. *Plasma Processes and Polymers*, 14(6):1600120, jun 2017.

[14] N. A. Dyatko, Y. Z. Ionikh, I. V. Kochetov, D. L. Marinov, A. V. Meshchanov, A. P. Napartovich, F. B. Petrov, and S. A. Starostin. Experimental and theoretical study of the transition between diffuse and contracted forms of the glow discharge in argon. *Journal of Physics D: Applied Physics*, 41(5):055204, mar 2008.

[15] C. M. Ferreira. Theory of a plasma column sustained by a surface wave. *Journal of Physics D: Applied Physics*, 14(10):1811–1830, 1981.

[16] A. Fridman. *Plasmas Chemistry*. Cambridge University Press, 2008.

[17] A. Fridman and L. A. Kennedy. *Plasma Physics and Engineering*. Taylor & Francis, New York, 2004.

[18] N. Gatti, S. Ponduri, F. J. J. Peeters, D. C. M. van den Bekerom, T. Minea, P. Tosi, M. C. M. van de Sanden, and G. J. van Rooij. Preferential vibrational excitation in microwave nitrogen plasma assessed by Raman scattering. *Plasma Sources Science and Technology*, 27(5):055006, may 2018.

[19] Y. B. Golubovskii, V. Nekuchaev, S. Gorchakov, and D. Uhrlandt. Contraction of the positive column of discharges in noble gases. *Plasma Sources Science and Technology*, 20(5):053002, oct 2011.

[20] P. W. C. Groen, A. J. Wolf, T. W. H. Righart, M. C. M. van de Sanden, F. J. J. Peeters, and W. A. Bongers. Numerical model for the determination of the reduced electric field in a CO 2 microwave plasma derived by the principle of impedance matching. *Plasma Sources Science and Technology*, 28(7):075016, jul 2019.

[21] a. Gutsol and J. a. Bakken. A new vortex method of plasma insulation and explanation of the Ranque effect. *Journal of Physics D: Applied Physics*, 31:704, 1998.

[22] E. W. Hansen and P.-L. Law. Recursive methods for computing the Abel transform and its inverse. *Journal of the Optical Society of America A*, 2(4):510, apr 1985.

[23] M. Heald and C. B. Wharton. *Plasma Diatnostics with Microwaves*. Wiley, 1965.

[24] Y. Kabouzi, M. D. Calzada, M. Moisan, K. C. Tran, and C. Trassy. Radial contraction of microwave-sustained plasma columns at atmospheric pressure. *Journal of Applied Physics*, 91(3):1008–1019, 2002.

[25] C. Kenty. Volume recombination, constriction and volt-ampere characteristics of the Positive Column. *The Physical Review*, 126(4):1235–1238, 1962.

[26] H.-J. Kunze. *Introduction to Plasma Spectroscopy*, volume 56 of *Springer Series on Atomic, Optical, and Plasma Physics*. Springer Berlin Heidelberg, Berlin, Heidelberg, 2009.

[27] H. S. Kwak, H. S. Uhm, Y. C. Hong, and E. H. Choi. Disintegration of Carbon Dioxide Molecules in a Microwave Plasma Torch. *Scientific reports*, 5:18436, 2015.

[28] E. C. Martinez, Y. Kabouzi, K. Makasheva, and M. Moisan. Modeling of microwave-sustained plasmas at atmospheric pressure with application to discharge contraction. *Physical Review E - Statistical, Nonlinear, and Soft Matter Physics*, 70(6 2):1–12, 2004.

[29] B. McBride, M. Zehe, and S. Gordon. NASA Glenn coeefficients for calculating thermodynamic properties of individual species. *NASA*, (NASA/TP-2002-211556):287, 2002.

[30] M. Moisan, C. M. Ferreira, Y. Hajlaoui, D. Henry, J. Hubert, R. Pantel, A. Ricard, and Z. Zakrzewski. Properties and applications of surface wave produced plasmas.

Revue de Physique Appliqu{é}e, 17(11):707–727, 1982.

[31] M. Moisan and J. Pelletier. *Physics of Collisional Plasmas*. Springer, Dordrecht, 2012.

[32] M. Moisan and Z. Zakrzewskit. Plasma sources based on the propagation of electromagnetic surface waves. *J. Phys. D: Appl. Phys*, 24:1025–1048, 1991.

[33] E. C. Neyts, K. Ostrikov, M. K. Sunkara, and A. Bogaerts. Plasma Catalysis: Synergistic Effects at the Nanoscale. *Chemical Reviews*, 115(24):13408–13446, 2015.

[34] G. M. Petrov and C. M. Ferreira. Numerical modeling of the constriction of the dc positive column in rare gases. *Physical Review E - Statistical Physics, Plasmas, Fluids, and Related Interdisciplinary Topics*, 59(3):3571–3582, 1999.

[35] Y. P. Raizer. *Gas discharge physics*. Springer-Verlag, Berlin, 1991.

[36] M. A. Ridenti, J. De Amorim, A. Dal Pino, V. Guerra, and G. Petrov. Causes of plasma column contraction in surface-wave-driven discharges in argon at atmospheric pressure. *Physical Review E*, 97(1):1–14, 2018.

[37] V. Rusanov, A. Fridman, and G. Sholin. The physics of a chemically active plasma with nonequilibrium vibrational excitation of molecules. *Uspekhi Fizicheskih Nauk*, 134(6):185, 1981.

[38] R. Snoeckx and A. Bogaerts. Plasma technology-a novel solution for CO2conversion? *Chemical Society Reviews*, 46(19):5805–5863, 2017.

[39] H. Sun, J. Lee, H. Do, S. K. Im, and M. Soo Bak. Experimental and numerical studies on carbon dioxide decomposition in atmospheric electrodeless microwave plasmas. *Journal of Applied Physics*, 122(3):1–11, 2017.

[40] Y. Tanaka, N. Yamachi, S. Matsumoto, S. Kaneko, S. Okabe, and M. Shibuya. Thermodynamic and transport properties of CO2, CO 2-O2, and CO2-H2 mixtures at temperatures of 300 to 30,000 K and Pressures of 0.1 to 10 MPa. *Electrical Engineering in Japan (English translation of Denki Gakkai Ronbunshi)*, 163(4):18–29, 2008.

[41] D. C. M. van den Bekerom, J. M. P. Linares, T. Verreycken, E. M. van Veldhuizen, S. Nijdam, G. Berden, W. A. Bongers, M. C. M. van de Sanden, and G. J. van Rooij. The importance of thermal dissociation in CO 2 microwave discharges investigated by power pulsing and rotational Raman scattering. *Plasma Sources Science and Technology*, 28(5):055015, may 2019.

[42] G. J. Van Rooij, H. N. Akse, W. A. Bongers, and M. C. Van De Sanden. Plasma for electrification of chemical industry: A case study on CO2 reduction. *Plasma Physics and Controlled Fusion*, 60(1), 2018.

[43] W. Wang and A. Bogaerts. Effective ionisation coefficients and critical breakdown electric field of CO2 at elevated temperature: Effect of excited states and ion kinetics. *Plasma Sources Science and Technology*, 25(5):055025, 2016.

[44] J. C. Whitehead. Plasma-catalysis: The known knowns, the known unknowns and the unknown unknowns. *Journal of Physics D: Applied Physics*, 49(24), 2016.

[45] A. J. Wolf, T. W. Righart, F. Peeters, P. W. C. Groen, R. Van de Sanden, and W. Bongers. Characterization of the CO₂ microwave plasma based on the phenomenon of skin depth-limited contraction. *Plasma Sources Science and Technology*, page submitted, oct 2019.

[46] A. Yang, Y. Liu, L. Zhong, X. Wang, C. Niu, M. Rong, G. Han, Y. Zhang, Y. Lu, and Y. Wu. Thermodynamic Properties and Transport Coefficients of CO2–Cu Thermal Plasmas. *Plasma Chemistry and Plasma Processing*, 36(4):1141–1160, 2016.

[47] H. Zhong, M. Shneider, M. S. Mokrov, and Y. Ju. Thermal-chemical instability of weakly ionized plasma in a reactive flow. *Journal of Physics D: Applied Physics*, page in press, aug 2019.